Modeling Urban Growth and Land-Use changes using GIS Based Cellular Automata: Case of Benslimane in Morocco

Benchelha, M.,[1] Benzha, F.[2] and Rhinane, H.[3]
Geosciences Laboratory, Faculty of Science Ain Chock, Km 8 El Jadida Road, B.P 5366 Maarif Casablanca 20100, Morocco, E-mail: benchelha.doc@gmail.com,[1] benzhafatiha@yahoo.fr,[2] h.rhinane@gmail.com[3]

Abstract
Sustainable urban planning and management require reliable land change models, which can be used to improve decision-making. Over the years, many urban growth models have been developed and used in the developed countries for forecasting growth patterns. In the developing countries, however, there exist a very few studies showing the application of these models and their performances. The study encompasses spatio-temporal land use/land cover (LULC) monitoring (1989–2019) and urban growth modelling (1999–2039) of Benslimane, Morocco to deduce the past and future urban growth paradigm and its influence on varied LULC classes integrating geospatial techniques and Cellular Automata (CA). The study focused on scrutinizing the reliability of the CA algorithm to function independently for urban growth modelling, provided with strong model calibration. For this purpose, satellite data of four stages of time at equal intervals along with the population density, the distance to the city center, the slope and the distance to the roads are used. The satellite-based LULC during 1989-2019 reported an increase of 3.8 Sq. Km (variation of 318%) between 1989 and 2019. The spatial variation analysis using the principal component analysis (PCA) technique exhibit high similarity in classification ranging from 89% to 91%. The projected LULC exhibit that the urban area will increase to 5,044 Sq. Km in 2019, primarily in the west and southwest parts. Between 2019-2039, urban growth will replace and transform other LULC (net loss of 1,364 Sq. Km), followed by vegetation cover (net loss of 0.345 Sq. Km).

1. Introduction

Urbanization is a significant symbol of the growth of science, technology, and the greater capacity of humanity to reform the natural world. It is also one of the required measures to modernize a country (He et al., 2011). In the local natural environment, the rapid development of urban areas has an impact on the complex socio-economic and natural systems, such as deforestation, air pollution, and agricultural land reduction (Jenerette et al., 2007 and Seto, 2011). To ensure sustainable urban growth (Hersperger et al., 2018) and to explicitly understand the spatial distribution of urban areas and spatio–temporal patterns, it is important to find an effective method to simulate and model urban expansion (Arsanjani et al., 2013, Poelmans and Van Rompaey, 2010 and Saadani et al., 2020). A variety of techniques and models have been developed over the last three decades to explain the dynamics of urban growth processes (Aburas et al., 2016 and Musa et al., 2017). The introduction of the geographic information system (GIS) into the modeling of urban expansion was important at the end of the 20th century (Batty et al., 1999 and Michalak, 1993), to understand the predictor variables of spatio–temporal changes. Regression models (Hu and Lo, 2007, Liao and Wei, 2014, Mom and Ongsomwang, 2016, Tahami et al., 2018 and Tayyebi and Pijanowski, 2014), including artificial neural networks (ANN)) (Mohammady and Delavar, 2016, Pijanowski et al., 2000, 2002, Pourebrahim et al., 2018, Tayyebi et al., 2011 and Tian et al., 2016), agent-based models (ABM) (Babakan and Taleai, 2015 and Hosseinali et al., 2013), are used for their efficient spatial computational capabilities. Cellular automata (CA) models are widely considered to be the most functional instruments (He et al., 2006, Li and Yeh, 2002, Shi and Pang, 2000, Tobler, 1970, Wu and Martin, 2002 and Zhang et al., 2011). Tobler first suggested the urban CA model in 1970, to simulate Detroit's urban growth. In San Francisco, (Clarke et al., 1997) simulated shifts in land use using the Slope Land use Exclusion Urbanization Transportation Hillshade (SLEUTH) CA model.

Batty and Xie (1994) researched urban sprawl in Baffalo using the CA model (Batty and Xie, 1994).

To research the urban growth of Guangzhou, (Wu, 2002) developed a logistic regression CA model. In northern China, (He et al., 2005) simulated land use shifts by integrating the model of system dynamics and the model of CA. The urban growth of Dongguan was simulated by (Li and Gar-On Yeh, 2004), using data mining and CA. (Li et al., 2012) applied the GPU technique to the CA model to simulate improvements in urban land use in the province of Guangdong. Mustafa et al., (2017) merged cellular automatons and agent-based approaches in Wallonia, Belgium, to model urban growth from 1990 to 2000. The urban planning of the cities of the Pearl River Delta was analyzed by (Liu et al., 2014) by combining the Landscape Expansion Index (LEI) and the CA model. In the last three decades, research using CA urban growth models have proliferated and provided in-depth insight into urban growth processes, which contributes to the development of urban growth strategies to ensure a sustainable urban future (Wu and Martin, 2002). The urban modeling and forecasting capabilities of CA models have been demonstrated and has been used successfully over the past fifteen years worldwide (Chaudhuri and Clarke, 2013). In this study, we aimed to examine the spatio–temporal dynamics of land use/land cover (LULC) over the past decades in order to model urban development for the municipality of Benslimane, Morocco using the CA algorithm. In this analysis, the LULC of four separate years: 1989, 1999, 2009, and 2019 was evaluated. In order to achieve this objective, we also considered other criteria and growth parameters, such as topography, road proximity, proximity to the city center, demographic statistics, as well as areas with growth constraints. The prediction of the future was useful in extrapolating the environmental effects of the urbanization of the town of Benslimane, which could help improve sustainability. In our analysis, we also report on the CA algorithm's accuracy and reliability in modeling the urban development of the city of Benslimane in Morocco. In recent decades, the urban area of Benslimane has expanded, so it seems appropriate to examine the urban growth trend and deduce its potential impact on other land use characteristics.

2. Study Area

The study was carried out in the municipality of Benslimane (Figure 1), capital of the agricultural province, bounded by the municipality of Ain Tizgha to the east and north, the municipality of Ziaida to the south and the municipality of Oulad Yahya Louta in the West. In the north-west, the high altitudes range from 175 to about 390 m. The area of the municipality of Benslimane is about 72 km^2, the polar coordinates are 33° 36N latitude and 7° 06W longitude, the Lambert coordinates averages are x = 342000, y = 336000. The town of Benslimane has a population of approximately 57101 inhabitants (RGPH 2014).
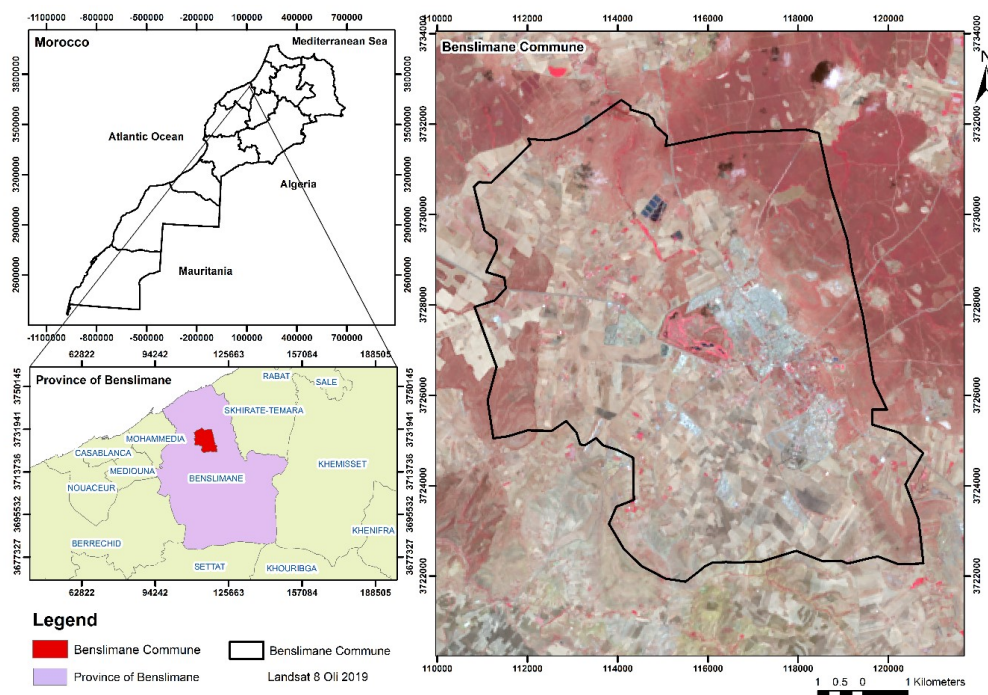

Figure 1: Map of the study area (Benslimane municipality)

The city of Benslimane is characterized by a dry climate with alternating cold and hot continental type (Benchelha et al., 2019). Benslimane's annual average temperatures are 23.7 °C for the maximum and 10.3 °C for the minimum. As one travels away from the Atlantic coast, there are considerable variations. The average annual temperature of the coastal zone is 17.5 °C, with a mean temperature not exceeding 32 °C. The low interior plateaus show very high thermal amplitudes, but without sudden variations. The average annual temperature on these plateaus is 18.5 °C, with a high of 40 °C (Benchelha et al., 2019). In the province, the average annual rainfall recorded is 350 mm. For the Feddan Taba and Malleh Dam pluviometry stations, the average annual precipitation measured for the period 1989–2019 is approximately 363 mm. The average monthly distribution of rainfall suggests the presence of two distinct seasons: the wet season from October to May, during which nearly all rainy episodes occurred (86 to 92% of the annual rainfall); the dry season from May to September, with just 8 to 14% of the annual rainfall (Benchelha et al., 2019).

3. Methods and Data Used

This research aims to prepare numerous thematic layers from satellite images..Different factors favoring urban growth with LULC were prepared as raster layers for modeling purposes, namely population density, Closeness of road networks, slope, and the city center's proximity (Figure 2). To achieve the best possible threshold values, a model has been carefully tuned to keep the simulated LULC statistically and spatially close to the real LULC. The trend of the obtained threshold values was assessed for future built-up projections for the years 2029 and 2039. The LULC, road network and other thematic layers were prepared in ArcGIS ver. 10.3, whereas calibration and future projection were conducted in Python 3.8, using GDAL 3.0.2, Numpy 1.18.1, Matplotlib 3.1.3, and Scikit-Learn 0.22.2 libraries.
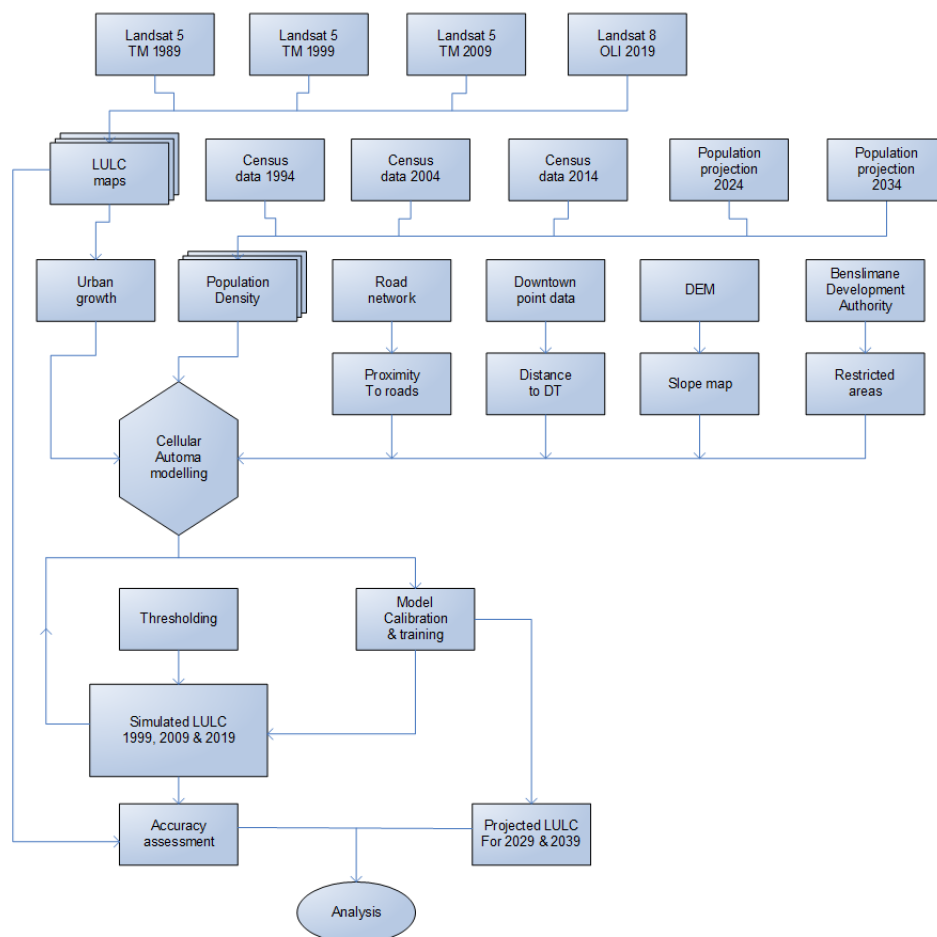

Figure 2: Procedures adopted in the study

3.1 Thematic Layers

LANDSAT multi-temporal satellite images for the years 1989, 1999, 2009, and 2019 were downloaded from the USGS website (https:/earthexplorer.usgs.gov) and were used to prepare LULC maps, using supervised classification on selected samples from different land use areas to obtain various groups: constructed, vegetation, water area, and others. The classification algorithm adopted here is a classification method based on maximum likelihood. Table 1 and Table 2 present a summary of the satellite data used and of the major LULC groups. The goal of this research was to design the built class of features, which includes built areas such as residential areas, institutions, informal settlements, and industries. Land was classified as vegetation primarily if it was under any form of green cover. Streams, etc., were included in the water zones, and the remainder was listed as other, mainly agricultural land. The satellite maps classified by the LULC were validated by the accuracy assessment method using randomly one hundred points as validation samples. These points were validated by a field check and Google Earth photos for the images between 2009 and 2019. In addition, the knowledge of the experts of the staff members of the local authorities including the regional directorate of forests, basin agency, commune of Benslimane and the old maps were used for the images of the years 1989 and 1999. For each of the observation years (1989, 1999, 2009 and 2019), the average accuracy was measured and ranged from 80 percent to 89 percent, while the coefficient of kappa ranged from 0.73 to 0.85.

Table 1: Input data specifics used in the analysis

Data type	Details	Date of acquisition
LANDSAT 5 TM	Path : 202 ; Row : 37	1989/08/07
LANDSAT 5 TM	Path : 202 ; Row : 37	1999/07/02
LANDSAT 5 TM	Path : 202 ; Row : 37	2009/06/27
LANDSAT 8 OLI	Path : 202 ; Row : 37	2019/06/23
Digital Elevation Model	ASTER Global Digital Elevation Model V003 (spatial resolution 30m)	2000-03-01
General Population and Housing Census	high commission for morocco plans	1994, 2004, 2014, 2024 and 2030

Table 2: Characteristics of land use/land cover maps (LULC) feature class

Feature class	characteristics	Description
Built-up	Consist of	All man-made structures that are primarily impervious including residential areas, commercial areas, with low economic relevance
	proximity	Parks, plantations, lakes, ponds, transport networks
	significance	high to moderate population density
Vegetation	Consist of	All green spaces and forests in the urban area and its surroundings, including agricultural land, parks, plantations, protected forests, agriculture
	proximity	Moderate to low built-up structures and water bodies
	significance	Public, private and government preserved area
Water	Consist of	All water bodies
	proximity	Low/high vegetation, open land
	significance	Potable/non-potable water, contaminated, irrigational
Other	Consist of	Toutes les caractéristiques à l'exclusion des constructions, de la végétation et de l'eau
	proximity	Low / high vegetation, built structures
	significance	Belonging to the private domain of the state and or to individuals

To examine LULC transition and urban sprawl over 1989–2019, and then to calibrate the model, the finalized LULC maps were adopted. The demographic data of the Moroccan census (1994, 2004 and 2014) were taken into account for the simulations and were used for the calibration of the model. and, for future forecasting purposes, the population density map for 2024-2030 was used. To accommodate the geometry of the other participating layers, the density was determined in the vector layer attribute of the different areas of Benslimane, which was then transformed into a 30 x 30 m raster layer. In all three groups (<3, 3–5,> 5), Digital Elevation Model (DEM) of spatial resolution 30 m acquired from USGS website (https:/earthexplorer.usgs.gov) was used to prepare the slope maps.

The main road network was obtained from the satellite picture showing proximity to the main roads, grading from 250 m by 3 km intervals Likewise, several buffer circles across the downtown location were sampled at 1 km intervals in 8 classes. The vector layers were rasterized at a cell size of 30m and cut to match the geometry of the old layers with constant magnitude. A layer for restriction zones was considered to improve the model's ability to reproduce the current growth system. The model did not produce pixels accumulated in restricted areas representing the forest and land inhabited by this binary layer.

3.2 Algorithm Model for CA
To take into account all the variables that lead to urban growth in Benslimane, a script has been formulated for the CA model. A kernel of 3*3 size kept the test pixel in its middle, as shown in Equation 1:

$$A_{ij}^t = \begin{bmatrix} a_{i-1j-1}^{(t)} & a_{i-1j}^{(t)} & a_{i-1j+1}^{(t)} \\ a_{ij-1}^{(t)} & a_{ij}^{(t)} & a_{ij+1}^{(t)} \\ a_{i+1j-1}^{(t)} & a_{i+1j}^{(t)} & a_{i+1j+1}^{(t)} \end{bmatrix} \quad \text{3*3neighbourhood}$$

Equation 1

The model primarily depends on the test pixel's current state, The current condition of the pixels that are immediately adjacent, and the set of transformation rules (Kumar et al., 2009). Matching layer geometry is important to ensure that in all raster layers, Any random pixel (ai, j) defines the same part of the terrain. According to equation (2), the dependence of the future state (t + 1) of the pixel on the passage rules (Ø) and the normal state of the pixel has been analyzed:

$$a_{i,j}^{t+1} = Ø\,(a_{i,j}^t)$$

Equation 2

The passing rules (φ) were a function of a set of threshold conditional statements represented by:

$$Ø=f\,(T,B)$$

Eqaution 3

Equation (3) suggests that the transition rules are a function of T, a set of threshold values for all the affected parameters, and B, a set of kernel count values associated with each set of T.

$$T= \{T_R, T_C, T_P, T_S\}$$

Equation 4

$$T= \{B_R, B_C, B_P, B_S\}$$

Equation 5

where the threshold values for road proximity, city center distance, population density, and slope value are TR, TC, TP, and TS, respectively; BR, BC, BP and BS are the corresponding number of pixels incorporated in the test kernel for each element belonging to T.

3.3 Calibrating the Mod
Model calibration was adopted to simulate the year 1999 using LULC satellite data for 1989, then LULC satellite data from 1999 to simulate the year 2009, and finally, LULC satellite data from 2009 to simulate the year. 2019. By simulating the LULC of time t2 using the LULC of time t1 and the driving parameters, the model deduced the best-defined threshold values, which represent the nearest result to the real world (Kumar et al., 2009), both statistically and spatially. The four factors' threshold values (TR, TC, TP, and TS) and their corresponding integrated pixel count values (BR, BC, BP and BS) were obtained through trial and error. Moreover, the script also tracked the contribution of each factor influencing the new integrated pixel generation. Threshold values were plotted after calibration, and trend lines were used to project thresholds for the future stage to estimate the extent of future accumulation (Tripathy, 2019).

For the sake of precision at each stage of the simulation, the PCA (principal component analysis) differencing method was used (Tripathy, 2019), where the difference between two images was determined by spatially subtracting the cumulative time pixels t2 from the corresponding time pixels t1.

Here, from satellite and simulated LULC images from the same time, dichotomous made up layers were extracted. In the event of a change, the built-up area common to the two images was eliminated by subtraction and generated non-zero values (1 or −1). For a precise percentage measure, the proportion of these non-zero values relative to the total number of pixels accumulated from satellite images was considered.

4. Results and Discussion
To infer the land use/land cover and urban sprawl trends for 1989-2019, LULC satellite images were prepared and analyzed. Later, to calibrate the model and project the future extent of the built environment, the main factors leading to urban growth were analyzed.

4.1 Mapping and Urban Development of Land Use/Land Cover
For 1989-2019, actual multi-temporary satellite data was used at 10-year intervals to map land use/land cover. The data was then used to simulate the LULC1999-2039. These simulations were associated with the actual LULC satellite during the model calibration period (1999 to 2019). We found that the actual built-up area (by satellite) increased from 1,206 to 5,044 km^2 in 1989-2019 with a variation of 5,305%. Periodic observations show that the built-up area in 1989 was 1,206 km^2 (1,667% of the total area), which increased to 2,147 km^2 (2,969%) in 1999 with an increase of 1,301% (Table 3). It increased to 2,999 km^2 (4,146%) in 2009 with an increase of 1,177%. In 2019, the built-up area increased to 5,044 km2 (6,972%) with a growth of 2,827%. The overall variation in the vegetation zone was observed at 6,464% between 1989 and 2019. In 1989, the vegetation cover covered 21,392 km^2 (29.57%) with a variation of 9,601%, which rose to 28,337 km^2 (39.17%) (1999).

It then increased in 2009 to 31,223 km^2 (43.16%) with a variance of 3.989%. In 2019, with a variation of −7.127%, the vegetation cover decreased to 26,068 km^2 (36.04%).

In the class of water characteristics from 1989 to 2019, the cumulative variation observed was 0.173%. In 1989, the area protected by water zones was 0.077 km^2 (0.106%), which increased to 0.266 km^2 (0.367%) with a variation of 0.261% in 1999. This area increased to 0.313 km^2 (0.433%)) in 2009 with a variation of 0.066%. In 2019, with a variation of -0.154%, the total area of water zones increased to 0.202 km^2 (0.279%). In the other class, the average decrease was -11,942%. In 1989, all remaining objects classified as other occupied a total area of 49.66 km^2 (68.65%), which decreased to 41.59 km^2 (57.49%) in 1999 with a variation of -11.164%. In 2009, with a difference of −5.232%, the area of the other class decreased to 37.80 km^2 (52.26%), then to 41.02 km^2 (56.71%) in 2019 with a difference of 4.454 %.

Our research illustrates the impact of urban sprawl from 1989 to 2019 on other LULC groups. LULC's spatio-temporal mapping shows that most of the built-up land was concentrated in the central region of Benslimane. Later, due to the availability of suitable sites and the adoption of the new development plan, the building was extended to the south and southwest, resulting in an increase in the population. Since built-up areas determine the basic dynamics between man and the environment, the unbuilt elements are intrinsic components of built-up areas (Figure 3).

4.2 Urban Expansion Modelling
4.2.1 Contributing factor in urban development
The study indicates that the densification and the formation of subdivisions in remote areas result from the impact of the restriction zone under the domain of habous.

Table 3: During 1989–2019, the LULC region statistics (satellite-based vs. simulated)

|	Type	Built-up land			Vegetation cover			Water body			Others		
		Area (km²)	%	Δ %	Area (km²)	%	Δ %	Area (km²)	%	Δ %	Area (km²)	%	Δ %
1989	Actual	1,206	1,667	-	21,392	29,57	-	0,077	0,106	-	49,66	68,65	-
1999	Actual	2,147	2,969	1,301	28,337	39,17	9,601	0,266	0,367	0,261	41,59	57,49	-11,164
	Simulated	2,330	3,221	1,554	28,104	38,85	9,278	0,255	0,352	0,246	41,67	57,61	-11,043
2009	Actual	2,999	4,146	1,177	31,223	43,16	3,989	0,313	0,433	0,066	37,80	52,26	-5,232
	Simulated	3,294	4,553	1,332	30,806	42,59	3,736	0,303	0,418	0,066	37,97	52,49	-5,125
2019	Actual	5,044	6,972	2,827	26,068	36,04	7,127	0,202	0,279	0,154	41,02	56,71	4,454
	Simulated	5,533	7,649	3,094	25,870	35,76	6,824	0,195	0,270	0,148	40,78	56,37	3,884
1989-2019	Actual	-	-	5,305	-	-	6,464	-	-	0,173	-	-	-11,942
	Simulated	-	-	5,982	-	-	6,190	-	-	0,164	-	-	-12,284
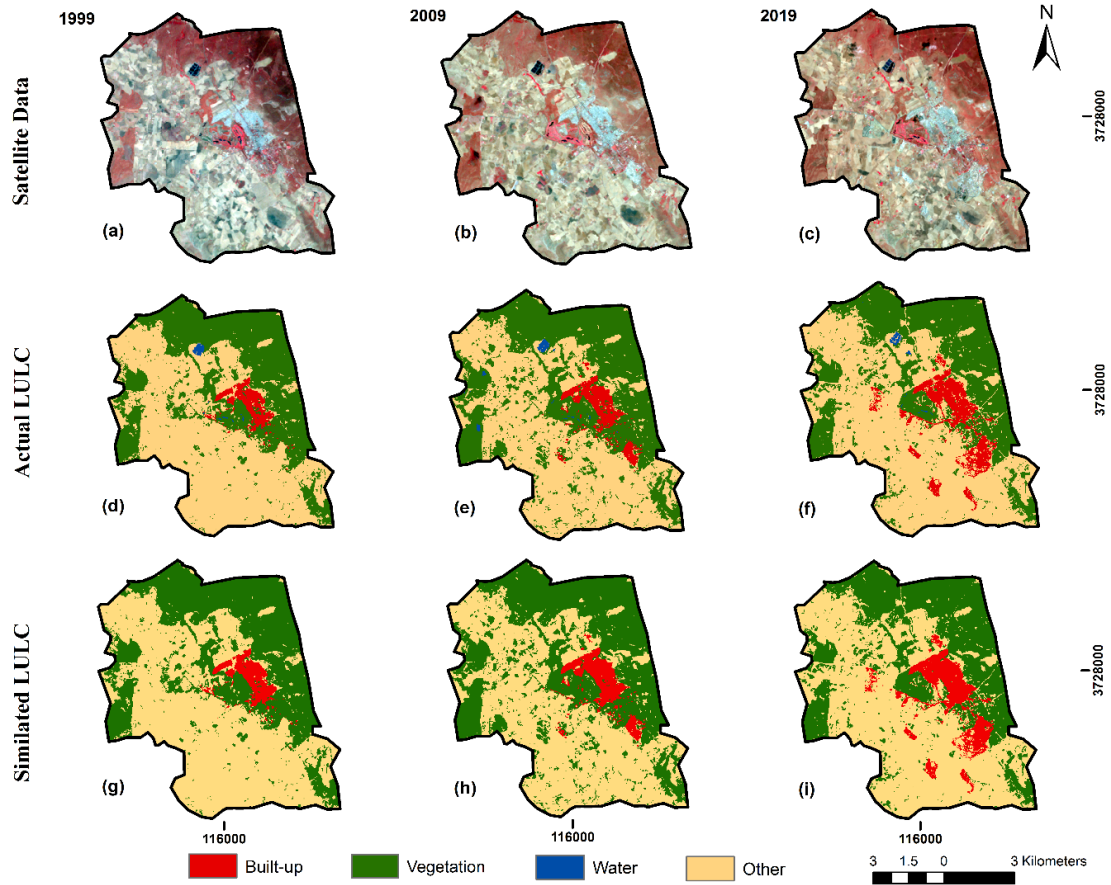
Figure 3: LANDSAT satellite images (a to c) (obtained from USGS), satellite-based LULC maps (d to f) and simulated LULC map (g to i) of Benslimane for the year 1999 (a, d, g), 2009 (b, e, h), and 2019 (c, f, i)

4.2.2 Land Use/Land Cover

The conversion of the different classes of LULC into built-up land is different. To this end, the other class was given a higher rank, followed by vegetation. In the modeling, the constructed land was planned as a non-transformable class.

4.2.3 Proximity to major roads

The road map shows the density of roads in the center and south of the city, and the density in the northwest and southwest is lower. Road density in most suburban areas is low (Figure 4a).

4.2.4 Slope

The analysis indicates that the relief varies between 177 and 339 m compared to the mean sea level (NGM) of Benslimane. The Benslimane slope map shows that most of the region has a slope of less than 5°, but small parts have slopes greater than 5° to the north, middle, southeast and southwest. (Figure 4c). The slope of the land is a factor which has a considerable influence on the growth of buildings. High landforms and steep slopes result in greater runoff and make the terrain less suitable for construction, while low landforms and gentle slopes provide buildings with a comparatively more stable foundation. This could explain why the growth of low slope areas has been favored

4.2.4 Population Density

In the early stages (1994-2014), in the middle of the city, in the south and the southeast, the population density map in Benslimane indicates a greater increase in density. The population density in the central zone remained> 15,000 inhabitants per km2 (Figure 5). Between 1994 and 2004, changes in population density were observed in the central western regions. The population density maps (2030) established by the High Commission for the Planning of Demographic Forecasting of Morocco indicate an increase in population density in the center-north, center-west and south-east, highlighting evidence of the future of Benslimane's expansion.
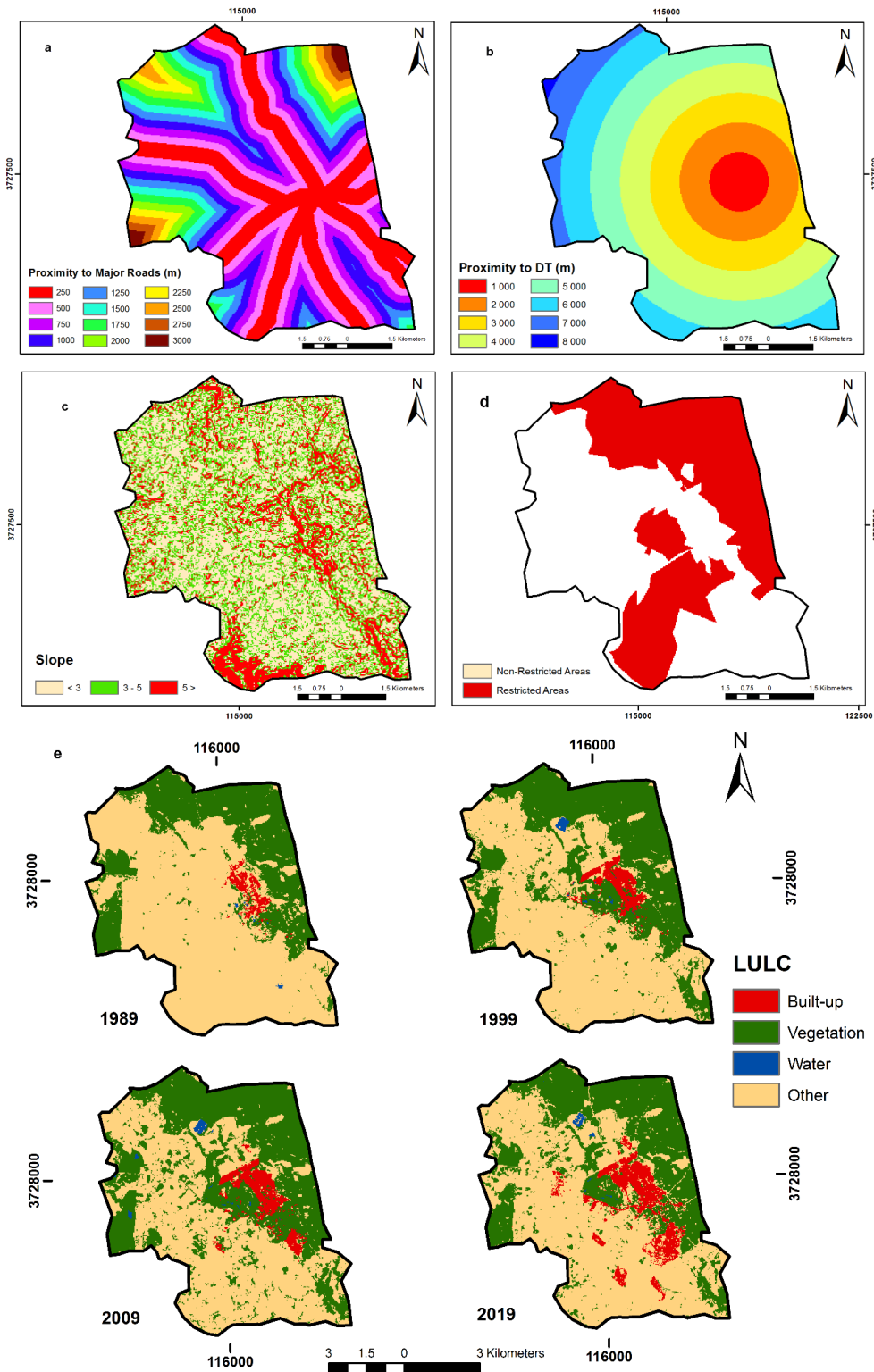
Figure 4: The leading factors to urban growth (a) proximity to major roads, (b) proximity to downtown, (c) digital elevation model (DEM) based slope map, (d) restricted areas, and (e) temporal satellite-based LULC classified images of 1989–2019 of Benslimane

4.3 Modeling of Urban Development using CA

As shown in Figure 6, The simulated construction was analogous to the actual construction for various years. Constructed land is expected to rise from 5,044 km^2 in 2019 to 6,092 km^2 in 2029. (20,789 % built growth) (Table 5), mostly in the city's west and south, and to 6,753 km^2 in 2039 (10,844 % built growth), with city core densification and scattered development predominantly in the western and southwestern sections. The coverage of vegetation will grow from 26,068 km^2 in 2019 to 25,889 km^2 in 2029 (-0.684% variation) and 25,723 km^2 in 2039 (-0.643% variation). It is expected that the area of the 'other' group will deteriorate, falling from 41,023 km2 in 2019 to 40,154 km^2 in 2029 and finally to 39,659 km2 in 2039 (Figure 7).
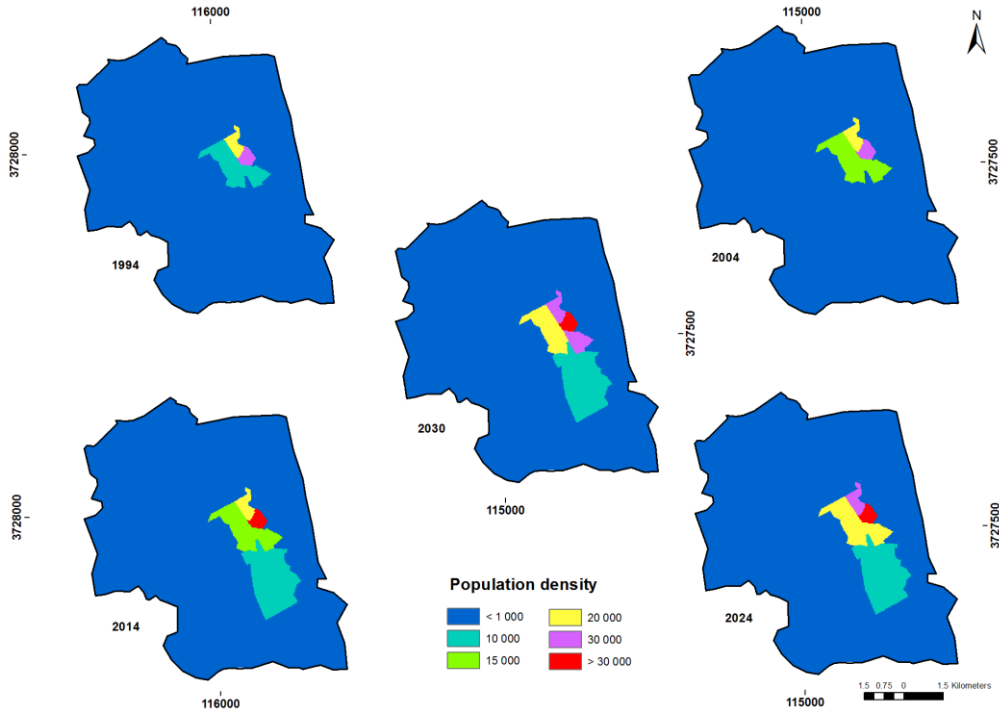

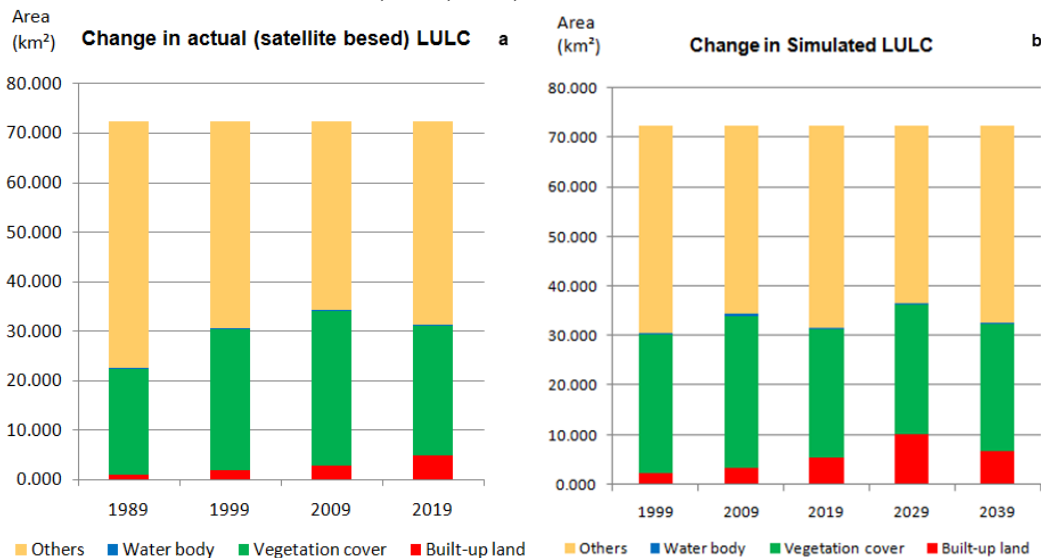Figure 5: Urban maps of Benslimane's population density for different times, 1994, 2004, 2014, 2020 and 2030

Figure 6: (a) A graph that shows the actual and (b) simulated LULC change

4.4 The Validation of the Simulated LULC

An evaluation of the precision showed a very high statistical and spatial similarity (> 89%) between the simulated LULC and the real LULC satellite for the known years (1999-2019) as shown in Table 4. The calculated confusion matrix was an overall accuracy of 97.23% (Table 6), and the area under the curve (AUC) of the receiver operating characteristics (ROC) graph (Figure 8) was found to be as high as 0.94. The high precision of the confusion matrix and the AUC indicates high accuracy of the modeling. This is probably due to the use of an average prediction period (10 years) at regular intervals during the calibration as well as to the proportion of built-up areas which represents only 7% of the total area. The transition matrix from 1989 to 2019 shown in Table 7 shows that most of the built pixels remained in the same class (0.960), and a very small number of built pixels were transformed into water (0.001) and class other (0.039), This may be due to misclassification caused by similar reflectance of elements as well as improved resolution of satellite data in recent years compared to previous years. A similar problem was observed in some areas of the water class which turned into built-up land (0.126) and other class (0.314). Likewise for the class other, certain areas have been transformed into buildings (0.302) and a small number into water class (0.018).

The transition matrix from 2019 to 2039 shown in Table 8 shows that the pixels of the built class have not changed (1). Pixels of the vegetation class turned into built-up terrain (0.148). The water class pixels have not received any changes (1). Pixels of the other class generated pixels of the built class (0.138).

4.5 Influence of Potential Urban Growth on Various LULC

An increase of 1,708 km² in urban areas and an urban growth rate of 33.88% between 2019 and 2039 was demonstrated by the built-up expansion illustrated by the urban growth model based on CA (Table 5). This will affect the other classes: loss of 1.32 km² of vegetation cover, loss of 0.44 km² of areas covered with water and loss of 3.32 km² of areas classified as other. Research shows that during the period 2019-2039, the urban growth rate in Benslimane will not be high.

Table 4: The statistical variability as per satellite-based and simulated photos of built-up land

Variables	Built-up areas in km²		
	1999	2009	2019
Actual (Km²)	2,147	2,999	5,044
Simulated (Km²)	2,330	3,294	5,533
Spatial accuracy	91,28	89,34	90,34

Table 5: Area statistics of varied classes for the year 2019 and projected 2029 and 2039 with the percentage change

	2019 (Km2)	2020 Km2	2039 Km2	% Change 2019-2039
Built-up	5,044	6,0921	6,7527	33,887
Vegetation	26,068	25,8894	25,7229	-1,322
Water	0,202	0,2007	0,2007	-0,446
Others	41,023	40,1535	39,6594	-3,324

Table 6: Confusion matrix for actual and simulated 2019 built-up pixels

		Predicted		Percentage correct	Overall accuracy
		Non-built-up	Built-up		
Actual	Nonbuilt-up	111491	3037	97.35%	
	Built-up	224	3108	93.28%	97.23%

Table 7: Transition matrix (satellite-based 1989 to 2019)

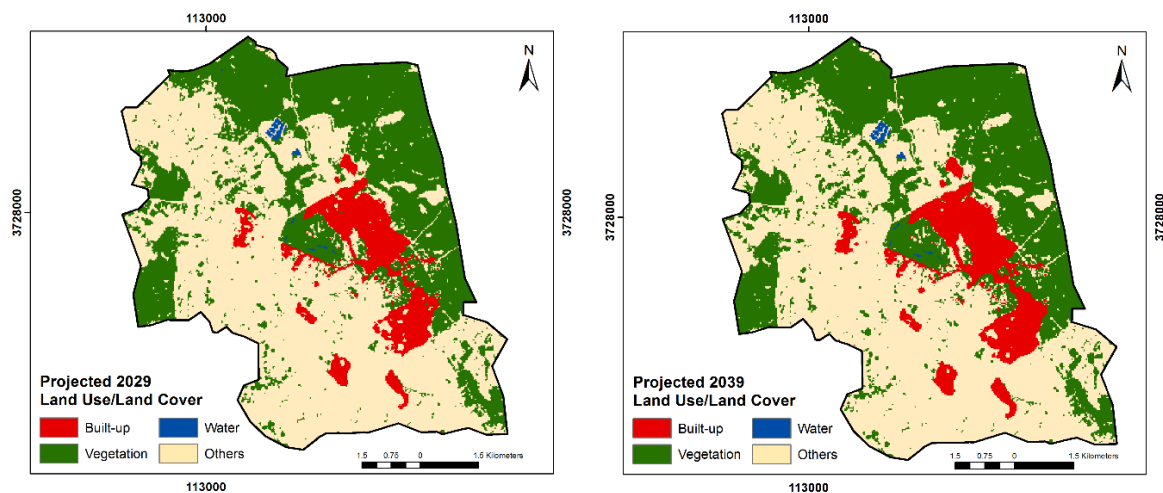| LULC	Built up	Vegetation	Water	Others
Built up	0.960	0	0.001	0,039
Vegetation	0.130	0,867	0	0,003
Water	0.126	0	0,560	0,314
Others	0,302	0	0,018	0,680

Figure 7: Cellular automata (CA) model-based simulated built-up growth for (a) 2029 and (b) 2039
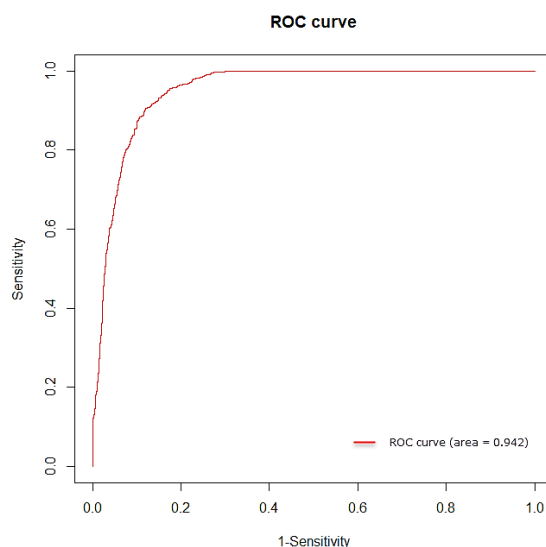

Figure 8: Receiver operating characteristic (ROC) curve for the actual and simulated built-up land during 2019

Table 8: Transition matrix (satellite-based 2019 to 2039)

	Built up	Vegetation	Water	Others
Built up	1	0	0	0
Vegetation	0,148	0,852	0	0
Water	0	0	1	0
Others	0,138	0	0	0,862

5. Conclusions

The research covers the spatio-temporal monitoring of the Benslimane LULC (1989-2019) and the modeling of urban growth (1999-2039) to study the effect of urban growth on the variety of land use / cover at using the CA model. During the period 1989-2019, the real and simulated LULC showed considerable urban growth (net increase of 3,838 km^2 and 4,327 km^2), resulting in a land use transition in Benslimane. The classe other have been modified by the urban growth: - 11.94% followed by the vegetation cover (6.46%) and the classe wate (0.173%). The simulated CA-based LULC shows that the urban area will expand from 5.044 to 6.09 km^2 in 2029 and 6.75 km^2 in 2039 mainly in the western and southwestern sectors. In the period

2019-2039, urban development will replace and transform the "other" category of LULC (loss of 1.36 km^2) and the category of vegetation cover (loss of 0.34 km^2). In the simulated and satellite LULC during the years described (1989–2019), the transition dynamics were parallel. For the years 1999 and 2019, the study of the spatial variance carried out using the PCA technique showed high construction precision. The overall precision of the confusion matrix (97.23%) and of the area under the receiver operational characteristics (ROC) curve (0.94) underlines the high precision of the modeling.

An attempt was made to demonstrate the relationship between variables related to the phase of spreading over time (1999–2039), which highlighted the strong impact over time of proximity to built-up areas and the city center during the initial observation period, although the population density contribution increased later .

References

Aburas, M. M., Ho, Y. M., Ramli, M. F. and Ash'aari, Z. H., 2016, The Simulation and Prediction of Spatio-Temporal Urban Growth Trends using Cellular Automata Models: A Review. *International Journal of Applied Earth Observation and Geoinformation*, Vol. 52, 380–389.

Arsanjani, J. J., Helbich, M., Kainz, W. and Boloorani, A. D., 2013, Integration of Logistic Regression, Markov chain and Cellular Automata Models to Simulate Urban Expansion. *International Journal of Applied Earth Observation and Geoinformation*, Vol. 21, 265–275.

Babakan, A. S. and Taleai, M., 2015, Impacts of Transport Development On Residence Choice Of Renter Households: An agent-Based Evaluation. *Habitat International*, Vol. 49, 275–285.

Batty, M. and Xie, Y., 1994, From Cells To Cities. *Environment and Planning B: Planning and Design*, Vol. 21(7), S31–S48.

Batty, M., Xie, Y. and Sun, Z., 1999, Modeling Urban Dynamics through GIS-based Cellular Automata. *Computers, Environment and Urban Systems*, Vol. 23(3), 205–233.

Benchelha, M., Benzha, F. and Rhinane, H., 2019, Object Based "Dayas" Classification Using Sentinel A-2 Satellite Imagery Case Study City of Benslimane. Int. Arch. Photogramm. Remote Sens. Spatial Inf. Sci., 33–39, https://doi.org/1-0.5194/isprs-archives-XLII-4-W12-33-2019.

Chaudhuri, G. and Clarke, K., 2013, The SLEUTH Land Use Change Model: A Review. *Environmental Resources Research*, Vol. 1(1), 88-105. https://doi.org/10.22069/ijerr.2013.1688.

Clarke, K. C., Hoppen, S. and Gaydos, L., 1997, A Self-Modifying Cellular Automaton Model of Historical Urbanization in the San Francisco Bay Area. *Environment and Planning B: Planning and Design*, Vol. 24(2), 247–261.

He, C., Okada, N., Zhang, Q., Shi, P. and Zhang, J., 2006, Modeling Urban Expansion Scenarios by Coupling Cellular Automata Model and System Dynamic Model in Beijing, China. *Applied Geography*, Vol. 26(3–4), 323–345.

He, C., Shi, P., Chen, J., Li, X., Pan, Y., Li, J., Li, Y. and Li, J., 2005, Developing Land Use Scenario Dynamics Model by the Integration of System Dynamics Model and Cellular Automata Model. *Science in China Series D: Earth Sciences*, Vol. 48(11), 1979–1989.

He, C., Tian, J., Shi, P. and Hu, D., 2011, Simulation of the Spatial Stress Due to Urban Expansion on the Wetlands in Beijing, China using a GIS-based Assessment Model. *Landscape and Urban Planning*, Vol. 101(3), 269–277.

Hersperger, A. M., Oliveira, E., Pagliarin, S., Palka, G., Verburg, P., Bolliger, J. and Grădinaru, S., 2018, Urban Land-Use change: The role of Strategic Spatial Planning. *Global Environmental Change*, Vol. 51, 32–42.

Hosseinali, F., Alesheikh, A. A. and Nourian, F., 2013, Agent-based Modeling of Urban Land-Use Development, Case Study: Simulating Future Scenarios of Qazvin City. *Cities*, Vol. 31, 105–113.

Hu, Z. and Lo, C. P., 2007, Modeling Urban Growth in Atlanta using Logistic Regression. *Computers, Environment and Urban Systems*, Vol. 31(6), 667–688.

Jenerette, G. D., Harlan, S. L., Brazel, A., Jones, N., Larsen, L. and Stefanov, W. L., 2007, Regional Relationships between Surface Temperature, Vegetation, and human Settlement in a Rapidly Urbanizing Ecosystem. *Landscape Ecology*, Vol. 22(3), 353–365.

Kumar, U., Mukhopadhyay, C., Ramachandra, T. V., Infrastructure, S. T. and Planning, U., 2009, Cellular Automata and Genetic Algorithms based Urban Growth Visualization for Appropriate Land Use Policies. *The Fourth Annual International Conference on Public Policy and Management, Centre for Public Policy*, 1-27, http://wgbis.ces.iisc.ac.in/energ-

y/paper/iimb_cellular_automata/cellular_automata.pdf.

Li, D., Li, X., Liu, X., Chen, Y., Li, S., Liu, K., Qiao, J., Zheng, Y., Zhang, Y. and Lao, C., 2012, GPU-CA Model for Large-Scale Land-Use Change Simulation. *Chinese Science Bulletin*, Vol. 57(19), 2442–2452.

Li, X. and Gar-On Yeh, A., 2004, Data Mining of Cellular Automata's Transition Rules. *International Journal of Geographical Information Science*, Vol. 18(8), 723–744.

Li, X. and Yeh, A. G. O., 2002, Neural-Network-Based Cellular Automata for Simulating Multiple Land Use changes using GIS. *International Journal of Geographical Information Science,* Vol. 16(4), 323–343.

Liao, F. H. and Wei, Y. D., 2014, Modeling Determinants of Urban Growth in Dongguan, China: A Spatial Logistic Approach. *Stochastic Environmental Research and Risk Assessment*, Vol. 28(4), 801–816.

Liu, X., Ma, L., Li, X., Ai, B., Li, S. and He, Z., 2014, Simulating urban Growth by Integrating Landscape Expansion Index (LEI) and Cellular Automata. I*nternational Journal of Geographical Information Science*, Vol. 28(1), 148–163.

Michalak, W. Z., 1993, GIS in Land Use Change Analysis: Integration of Remotely Sensed Data into GIS. *Applied Geography*, Vol. 13(1), 28-44.

Mohammady, S. and Delavar, M. R., 2016, Urban Sprawl Assessment and Modeling Using Landsat Images and GIS. Modeling Earth Systems And Environment, Vol. 2(3), 1-14, DOI:10.1007-/s40808-016-0209-4.

Mom, K. and Ongsomwang, S., 2016, Urban Growth Modeling of Phnom Penh, Cambodia Using SaᵀᴱᴸLite Imageries and a Logistic Regression Model. S*uranaree Journal of Science & Technology*, Vol. 23(4). 1-20.

Musa, S. I., Hashim, M. and Reba, M. N. M., 2017, A Review of Geospatial-Based Urban Growth Models and Modelling Initiatives. *Geocarto International*, Vol. 32(8), 813–833.

Mustafa, A., Cools, M., Saadi, I. and Teller, J., 2017, Coupling Agent-Based, Cellular Automata and Logistic Regression Into A Hybrid Urban Expansion Model (HUEM). *Land Use Policy*, Vol. 69, 529–540.

Pijanowski, B. C., Brown, D. G., Shellito, B. A. and Manik, G. A., 2002, Using Neural Networks and GIS to Forecast Land Use Changes: A Land Transformation Model. *Computers, Environment and Urban Systems*, Vol. 26(6), 553–575.

Pijanowski, B. C., Gage, S. H., Long, D. T. and Cooper, W. C., 2000, A Land Transformation Model: Integrating Policy, Socioeconomics and Environmental Drivers Using a Geographic Information System. *Landscape Ecology: A Top down Approach*, 183–198.

Poelmans, L. and Van Rompaey, A., 2010, Complexity and Performance of Urban Expansion Models. *Computers, Environment and Urban Systems*, Vol. 34(1), 17–27.

Pourebrahim, N., Sultana, S., Thill, J.-C. and Mohanty, S., 2018, Enhancing Trip Distribution Prediction with Twitter Data: Comparison of Neural Network and Gravity Models. *Proceedings of the 2nd ACM SIGSPATIAL International Workshop on AI for Geographic Knowledge Discovery*, 5–8.

Saadani, S., Laajaj, R., Maanan, M., Rhinane, H. and Aaroud, A., 2020, Simulating Spatial–Temporal Urban Growth of a Moroccan Metropolitan Using CA–Markov Model. *Spatial Information Research*, Vol. 28(5), 609–621. https://doi.org/10.1007/s41324-020-00322-0.

Seto, K. C., 2011, Exploring the Dynamics of Migration to Mega-Delta Cities in Asia and Africa: Contemporary Drivers and Future Scenarios. *Global Environmental Change,* Vol. 21, S94–S107.

Shi, W. and Pang, M. Y. C., 2000, Development of Voronoi-Based Cellular Automata-An Integrated Dynamic Model for Geographical Information Systems. *International Journal of Geographical Information Science*, Vol. 14(5), 455–474.

Tahami, H., Basiri, A., Moore, T., Park, J. and Bonenberg, L., 2018, Virtual Spatial Diversity Antenna for GNSS Based Mobile Positioning in the Harsh Environments. *Proceedings of the 31st International Technical Meeting of the Satellite Division of The Institute of Navigation (ION GNSS+ 2018)*, 3186–3198.

Tayyebi, A. and Pijanowski, B. C., 2014, Modeling Multiple Land Use Changes Using ANN, CART and MARS: Comparing Tradeoffs in Goodness of Fit and Explanatory Power of Data Mining Tools. *International Journal of Applied Earth Observation and Geoinformation*, Vol. 28, 102–116.

Tayyebi, A., Pijanowski, B. C. and Tayyebi, A. H., 2011, An Urban Growth Boundary Model using Neural Networks, GIS and Radial Parameterization: An Application to Tehran, Iran. *Landscape and Urban Planning*, Vol. 100(1–2), 35–44.

Tian, G., Ma, B., Xu, X., Liu, X., Xu, L., Liu, X., Xiao, L. and Kong, L., 2016, Simulation of

Urban Expansion and Encroachment Using Cellular Automata and Multi-Agent System Model-A Case Study of Tianjin Metropolitan Region, China. *Ecological Indicators*, Vol. 70, 439–450.

Tobler, W. R., 1970, A Computer Movie Simulating Urban Growth in the Detroit Region. *Economic Geography*, Vol. 46(sup1), 234–240.

Tripathy, P., 2019, Monitoring and Modelling Spatio-Temporal Urban Growth of Delhi using Cellular Automata and geoinformatics. *Cities*, Vol. 90, 52-63.

Wu, F., 2002, Calibration of Stochastic Cellular Automata: The Application to Rural-Urban Land Conversions. *International Journal of Geographical Information Science*, Vol. 16(8), 795–818.

Wu, F. and Martin, D., 2002, Urban Expansion Simulation of Southeast England using Population Surface Modelling and Cellular Automata. *Environment and Planning A*, Vol. 34(10), 1855–1876.

Zhang, Y., Li, X., Liu, X. and Qiao, J., 2011, The CA Model Based on Data Assimilation. *Journal of Remote Sensing*, Vol. 15(3), 475–491.